

Received January 11, 2020, accepted February 1, 2020, date of publication February 11, 2020, date of current version February 20, 2020.

Digital Object Identifier 10.1109/ACCESS.2020.2973281

Parameter Setting Strategy for the Controller of the DFIG Wind Turbine Considering the Small-Signal Stability of Power Grids

YANBING JIA¹, (Member, IEEE), TAO HUANG^{1,2,3}, (Member, IEEE),
YUBO LI⁴, AND RONGRONG MA¹

¹Shanxi Key Laboratory of Power System Operation and Control, Taiyuan University of Technology, Taiyuan 030024, China

²Department of Energy, Politecnico di Torino, 10129 Turin, Italy

³School of Electrical Engineering and Electronic Information, Xihua University, Chengdu 610039, China

⁴Yuncheng Power Supply Company, State Grid Corporation of China, Yuncheng 044000, China

Corresponding author: Tao Huang (tao.huang@polito.it)

This work was supported in part by the National Natural Science Foundation of China under Grant 51877181 and Grant 51807129, and in part by the Key R&D Plan of Shanxi Province (International Cooperation) under Grant 201803D421010.

ABSTRACT Due to the increasing penetration of the wind generation, the stability, especially the small-signal stability, of the power grid is much related to it. Currently, few studies considered the impact of the parameter settings of the wind turbine controller on the small-signal stability of the grid under the full range of wind conditions. In this paper, we propose a framework for deriving a set of controller parameters by interiorizing their impact on the power system stability, based on an analytic model of a 15th-order single DFIG-infinite grid connection under all wind speeds. The study results on a real wind turbine show that the controller parameters optimized for a specific wind speed may not feasible for other operational conditions yet the proposed framework can obtain a set of parameters guaranteeing the power system stability under all wind speeds.

INDEX TERMS Wind turbine with doubly-fed induction generator, small-signal stability, controller parameters setting, direct power control.


I. INTRODUCTION

The energy transition and environmental concerns require the generation of electricity from clean and renewable sources, therefore, the wind has become the world's fastest-growing energy source. Among different wind harvest technologies, the doubly-fed induction generators (DFIGs) have become the mainstream of wind turbines (WT) in the past several decades [1].

The DFIG WT control system includes back-to-back converter controller, pitch angle controller and phase-locked loop controller [2], which contain several PI links, thus the stability of its grid-connected system is closely related to the control parameters and corresponding control strategy. Small-signal stability issue of the grid, caused by the large-scale connected DFIG WT, is increasingly serious [3], [4]. Therefore, how to set the parameters of the control system of the DFIG WT to ensure the small-signal stability of the power grid has become

an urgent problem to be solved. However, the traditional controller parameters design method determines the feasible range of each control parameter by the classical control theory without considering the small-signal stability of power grids [5].

In order to analyze the impact of the wind power integration on the small-signal stability of the power system, researchers have established a small-signal model of the WT DFIG system in [6]–[8], in which the converter controller strategy just adopts the vector-oriented control strategy, and the main focus is the influence of generator electrical parameters and WT mechanical parameters on system's small-signal stability. In recent years, the direct power control (DPC) strategy of the WT with DFIG back-to-back converter has gradually become a research hotspot due to its simple structure and good dynamic performance [9]–[11], however, it has more controller parameters to be tuned to maintain the stability of power system. In [11], the participation factors are used to identify the dynamic mode which describes the association between the eigenvalues and state variables of

The associate editor coordinating the review of this manuscript and approving it for publication was Tariq Masood .

linear dynamic systems. In [12], a mathematical model of the DFIG and the power system is established to simulate the stability of the power system with variable wind speeds, but the model cannot obtain parameters that can guarantee the system stability.

In general, for the existing studies, most of them focused on verifying the system stability with different wind speeds and electrical parameters without considering the controller parameters setting strategy to increase the stability of the power grid under the whole range of wind speed. Therefore, in this paper, the small-signal stability characteristics of the grid integrating the DFIG WT system controlled by the DPC are analyzed in-depth, and the controller parameter setting strategy is proposed to improve the stability of the power grid based on a derived 15th-order analytic model of a common DFIG WT with an infinite bus system. By the Lyapunov small-signal stability analysis method, the correlation between the small-signal stability of the power grid and the control system parameters under all possible wind speed conditions is studied. Through the analysis of the small-signal stability under full wind speed, a universal set of parameters of the controller setting strategy is determined. Taking a DFIG WT with an infinite bus as an example, the effect of the WT control system parameters on the power grid small-signal stability under different wind speeds are analyzed in detail, which verifies the effectiveness and practicability of the proposed strategy.

The rest of the paper is organized as follows. In Section II, three operation modes of the WT are discussed. In Section III, a small-signal stability analysis model of the DFIG WT is briefly introduced. In Section IV, the corresponding state equations are derived. In Section V, the theoretical basis and implementation steps of the parameters setting strategy of the controller used in the DFIG WT are proposed. A real example of a 2 MW wind turbine in the Laoqian Shan wind farm in Shanxi Province is studied in Section VI. Finally, some conclusions are drawn in Section VII.

II. THREE OPERATION MODES OF THE WT

A sketch of relationships among the output power P of a DFIG WT, WT rotor speed ω_{tur} and pitch angle β versus wind speed is shown in Fig. 1. According to the variation of the wind speed, the operating characteristics of the WT can be divided into three different zones (AB, BC, CD). Point A corresponds to the cut-in wind speed, Point B corresponds to the constant rotating speed, point C corresponds to the rated wind speed, and point D corresponds to the cut-out wind speed.

- Zone AB – where the energy capture is optimized. The energy optimization is achieved by tracking the maximum wind power coefficient C_p^{max} through the rotating speed adjustment.
- Zone BC – where the WT rotor speed is limited to the rated value, i.e. $\omega_{tur} = \omega_{tur}^{rated}$.
- Zone CD – where the energy capture is limited. This mode corresponds to the situation when the wind speed

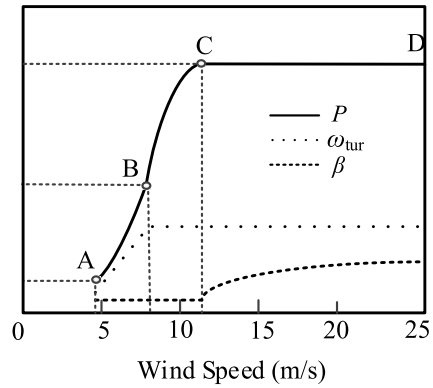


FIGURE 1. Three operation zones of a DFIG WT.

is larger than the rated wind speed and less than the cut-out wind speed, i.e. $V^{rated} \leq V \leq V_{out}$. The output power of the DFIG WT is then set to the rated value, i.e. $P = P^{rated}$, by the operation of the pitch angle control.

The mechanical power P_m captured by the WT can be expressed by equation (1):

$$P_m = \begin{cases} \frac{1}{2} \rho \pi R^5 \frac{C_p^{max}}{\lambda_{opt}^3} (\omega_{tur}^{ref})^3 & \text{zone AB} \\ \frac{1}{2} \rho \pi R^5 \frac{C_p}{\lambda(V)^3} (\omega_{tur}^{nom})^3 & \text{zone BC} \\ P_m^{norm} & \text{zone CD} \end{cases} \quad (1)$$

$$\omega_{tur}^{ref} = \frac{\lambda_{opt} V}{R} \quad (2)$$

where ω_{tur}^{ref} is the reference angle speed, λ is the blade tip speed ratio, λ_{opt} is the optimum tip speed ratio, V is the wind speed, ω_{tur} is the WT angle speed, R is the WT blade radius, ρ is the air density, and C_p is the wind energy utilization factor.

III. MATHEMATICAL MODELS OF THE DFIG WT

The mathematical models of the DFIG WT include the WT shafting model, doubly-fed induction generators model, DC capacitors model, and control system model. Fig. 2 illustrates the structure of a double-fed turbine with an infinite bus system. The power and current reference directions for each branch are shown in Fig. 2.

A. MODEL OF THE DRIVE TRAIN

The drive train uses the two-mass model [4], given by (3)-(5).

$$2H_{tur} \frac{d\omega_{tur}}{dt} = T_M - K_s \theta_s - D_s (\omega_{tur} - \omega_r) \quad (3)$$

$$2H_{gen} \frac{d\omega_r}{dt} = K_s \theta_s + D_s (\omega_{tur} - \omega_r) - T_e \quad (4)$$

$$\frac{d\theta_s}{dt} = \omega_0 (\omega_{tur} - \omega_r) \quad (5)$$

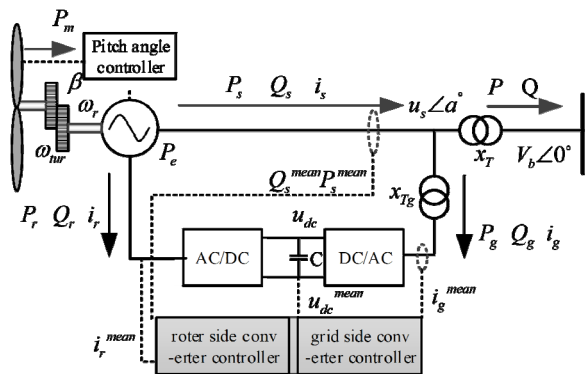


FIGURE 2. The double-fed wind turbine connected to an infinite bus.

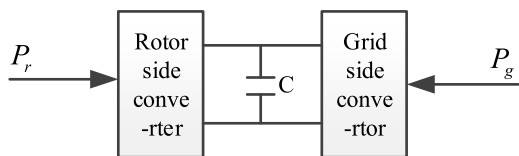


FIGURE 3. Model of the DC capacitor.

where H_{tur} and H_{gen} are the inertia constants of the WT and the generator, respectively, θ_s is the shaft twist angle, ω_{tur} and ω_r are the angle speeds of the WT and the generator rotor, respectively, ω_0 is the angle speed base of the system, D_s is the damping coefficient, K_s is the shaft stiffness, T_e is the electromagnetic torque.

B. THE DFIG SYSTEM MODEL

The DFIG system model uses a second-order model that ignores the transient process of the stator:

$$\frac{dE_d}{dt} = -\omega_1 \frac{L_m}{L_r} u_{rd} - \omega_1 \frac{R_r}{L_r} E_d + s\omega_1 E_q + \omega_1 R_r \frac{L_m^2}{L_r^2} i_{sd} \quad (6)$$

$$\frac{dE_q}{dt} = \omega_1 \frac{L_m}{L_r} u_{rd} - \omega_1 \frac{R_r}{L_r} E_q - s\omega_1 E_d - \omega_1 R_r \frac{L_m^2}{L_r^2} i_{sd} \quad (7)$$

where E_d and E_q are the d and q axis voltages behind the transient reactance, respectively, L_r is the rotor self-inductance, L_m is the mutual inductance, R_r is the rotor resistance, ω_1 is synchronous angle speed, s is the rotor slip, u_{rd} , and u_{rq} are the d and q axis rotor terminal voltage, respectively, i_{sd} and i_{sq} are the d and q axis stator-side current, respectively.

C. THE DYNAMIC MODEL OF THE DC CAPACITOR

$$cu_{dc} \frac{du_{dc}}{dt} = P_r + P_g = u_{rd}i_{rd} + u_{rq}i_{rq} + (u_{gd}i_{gd} + u_{gq}i_{gq}) \quad (8)$$

where i_{rd} and i_{rq} are the d and q axis current, respectively.

D. THE CONTROL SYSTEM MODEL

1) THE ROTOR-SIDE CONVERTER CONTROLLER MODEL

The rotor-side converter control strategy uses direct power control, and the control block diagram is shown in Fig. 4.

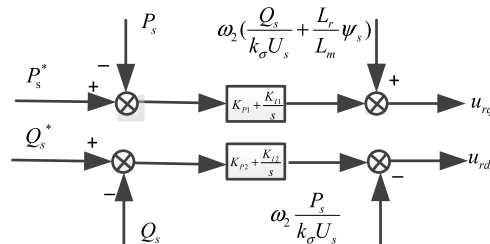


FIGURE 4. The diagram of the rotor-side inverter controller.

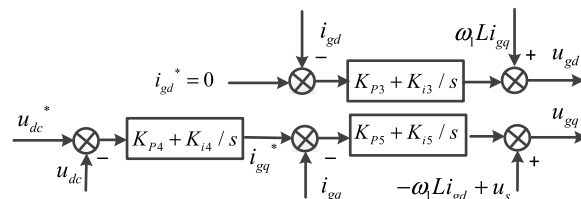


FIGURE 5. The grid-side inverter controller diagram.

Two state variables x_1, x_2 have been introduced, and control equations are given by (9)-(13).

$$\frac{dx_1}{dt} = P_s^* - P_s \quad (9)$$

$$u_{rq} = K_{P1}(P_s^* - P_s) + K_{I1}x_1 + \omega_2 \left(\frac{Q_s}{k_\sigma U_s} + \frac{L_r}{L_m} \psi_s \right) \quad (10)$$

$$\frac{dx_2}{dt} = Q_s^* - Q_s \quad (11)$$

$$u_{rd} = K_{P2}(Q_s^* - Q_s) + K_{I2}x_2 - \omega_2 \frac{P_s}{k_\sigma U_s} \quad (12)$$

$$k_\sigma = \frac{L_m}{L_s L_r - L_m^2} \quad (13)$$

where the superscript * indicates the reference value, P_s and Q_s are the stator side active and reactive power values, u_{rd} and u_{rq} are the d and q axis rotor voltage, respectively, ψ_s is the stator flux linkage, U_s is the amplitude of the terminal voltage. K_{Pi} and K_{Ii} ($i = 1, 2$) are proportional and integrating parameters, respectively, L_s is the stator self-inductance.

2) THE GRID-SIDE CONVERTER CONTROLLER MODEL

The grid-side converter control strategy uses stator voltage-oriented control, and the control block diagram is shown in Fig. 5. The stator voltage is oriented with the q axis and set i_{gd}^* to zero, which can limit reactive power exchanged between the grid-side converter and the system to zero. Three state variables x_3, x_4, x_5 have been introduced, and control equations are given by (14)-(19).

$$\frac{dx_3}{dt} = i_{gd}^* - i_{gd} \quad (14)$$

$$u_{gd} = K_{P3} (i_{gd}^* - i_{gd}) + K_{I3}x_3 \quad (15)$$

$$\frac{dx_4}{dt} = i_{dc}^* - u_{dc} \quad (16)$$

$$i_{gq}^* = K_{P4}(u_{dc}^* - u_{dc}) + K_{I4}x_4 \quad (17)$$

$$\frac{dx_5}{dt} = i_{gq}^* - i_{gq} = K_{P4}(u_{dc}^* - u_{dc}) + K_{I4}x_4 - i_{gq} \quad (18)$$

$$u_{gq} = K_{P5}[K_{P4}(u_{dc}^* - u_{dc}) + K_{I4}x_4 - i_{gq}] + K_{I5}x_5 - x_{Tg}i_{gd} + U_s \quad (19)$$

where i_{gd} and u_{gd} are the d-axis components of the grid-side converter current and voltage. i_{gq} and u_{gq} are the q-axis components of the converter current and voltage, u_{dc} is the capacitor terminal voltage. x_{Tg} is the equivalent reactance of the transformer on the grid side of the back-to-back converter. K_{Pi} and K_{Ii} ($i = 3, 4, 5$) are the proportional and integration parameters of the PI block, respectively.

3) THE PITCH ANGLE CONTROL MODEL

The pitch angle control can improve the efficiency of wind energy conversion and limit the output power [2]. The mathematical model is given by (20)-(22).

$$\frac{d\beta}{dt} = \frac{1}{T_{servo}}(\beta_0 - \beta) \quad (20)$$

$$\beta_0 = K_{P\beta}(P - P_{ref}) + K_{I\beta}x_\beta \quad (21)$$

$$\frac{dx_\beta}{dt} = P - P_{ref} \quad (22)$$

where $K_{P\beta}$ and $K_{I\beta}$ are the proportional and integration parameter of the PI block, and state variable x_β have been introduced. β is the pitch angle, T_{servo} is the inertia time constant, P_{ref} is the output power reference value.

4) THE PHASE-LOCKED LOOP CONTROLLER MODEL

The DFIG WT uses the phase-locked loop control to obtain the frequency, phase, and voltage amplitude of the power grid to achieve synchronization between the WT and grid [15]. The mathematical model is given by (23)-(24).

$$\frac{dx_6}{dt} = \Delta u_{sq} \quad (23)$$

$$\frac{d\theta_p}{dt} = K_{P6}\Delta u_{sq} + K_{I6}x_6 \quad (24)$$

where K_{P6} and K_{I6} are the proportional and integration parameters of the PI block, and state variable x_6 has been introduced. u_{sq} is the q axis stator voltage, θ_p is the output phase of the phase-locked loop.

IV. STATE EQUATION OF THE SINGLE DFIG-INFINITE SYSTEM

According to the flow direction of each electrical quantity in Fig. 2, the voltage at the grid connection point is given by (25).

$$V_s \angle \alpha = V_b \angle 0 + jx_T I^{\&} \quad (25)$$

The voltages at the d-q axes are given by (26)-(27).

$$u_{sd} = V_b \cos \alpha - x_T(i_{sq} - i_{gq}) \quad (26)$$

$$u_{sq} = -V_b \sin \alpha + x_T(i_{sd} - i_{gd}) \quad (27)$$

where u_{sd} and u_{sq} are the d and q axis stator voltage, respectively.

The grid-side converter voltages are given by (28)-(29).

$$u_{sd} - u_{gd} = -x_{Tg}i_{gq} \quad (28)$$

$$u_{sq} - u_{gq} = x_{Tg}i_{gd} \quad (29)$$

The power for the grid-side converters and the output powers of the stator of the DFIG are given by (30)-(33), respectively:

$$P_g = u_{gd}i_{gd} + u_{gq}i_{gq} \quad (30)$$

$$Q_g = u_{gq}i_{gd} - u_{gd}i_{gq} \quad (31)$$

$$P_s = u_{sd}i_{sd} + u_{sq}i_{sq} \quad (32)$$

$$Q_s = u_{sq}i_{sd} - u_{sd}i_{sq} \quad (33)$$

State variables and input variables are given by (34).

$$\begin{cases} x = [\beta, x_\beta, \omega_{nr}, s, \theta_s, E_d, E_q, x_1, x_2, x_3, x_4, x_5, x_6, \theta_p, u_{dc}]^T \\ y = [i_{rd}, i_{rq}, i_{gd}, i_{gq}]^T \end{cases} \quad (34)$$

For the state equations (3)-(33), the corresponding input equation is established by the flux linkage equation and the voltage equation of the DFIG [16]. When the WT is in different operating zones, their output characteristics are quite different. Therefore, three groups of state equations and input equations are established respectively in three operation zones. Three sets of state equations and the input equations are further linearized at their equilibrium points by using the Lyapunov linearization method.

$$\Delta x' = A' \Delta x + B \Delta y \quad (35)$$

$$C \Delta x + D \Delta y = 0 \quad (36)$$

Small-signal stability analysis model of the WT with DFIG can be obtained as follows

$$\Delta x' = A \Delta x \quad (37)$$

where $A = A' - BD^{-1}C$ is the system state matrix. The detailed derivation is given in Appendix A.

For the eigenvalue $\lambda = \sigma \pm j\omega$ of matrix A , the real part σ depicts the damping of the system, and the imaginary part ω indicates the oscillation frequency of the grid. Therefore, to increase the oscillation damping and reduce the oscillation period, we want a large $|\sigma|$ and small ω .

Further, to quantitatively evaluate the contribution of the σ and ω to the small-signal stability, we define a stability margin Y_i of λ_i as

$$Y_i = -\text{Re}(\lambda_i) - |\text{Im}(\lambda_i)| \quad (38)$$

Then an index of the small-signal stability margin of the grid can be defined as

$$Y = \sum_{i=1}^N Y_i \quad (39)$$

where N is the order of the system. It is obvious that the larger Y the more robust of the grid. Yet the equation (39) cannot guarantee that the real parts of all eigenvalues are negative. Therefore, the real parts of all eigenvalues should satisfy:

$$\text{Re}(\lambda_i) < C < 0 \quad (i = 1, 2, \dots, N) \quad (40)$$

where C is the stability threshold to guarantee enough stability margin.

To make Y as large as possible, the participation factor is commonly used to describe the sensitivity between the control parameters and the eigenvalues, i.e. though the sensitivity analysis, we can find the best way to set the control parameters to enlarge the stability margin. The participation factor p_{ki} of the k -th variable x_k of λ_i can be defined as [15]:

$$p_{ki} = u_{ki}v_{ki} \quad (41)$$

where u_{ki} and v_{ki} are the k -th row and the i -th column elements of the left and right characteristic vectors of A , respectively. The larger the module value of the p_{ki} , the greater correlation between the state variable x_k and the mode λ_i , which can be used to describe the relativity between each eigenvalue and the control parameters $K_{p1} \sim K_{p6}, K_{p\beta}$.

V. CONTROL SYSTEM PARAMETER SETTING STRATEGY

When the wind speed is higher than the rated wind speed, the output power of the WT and the related characteristic equation does not change with the wind speed (zone CD in Fig. 1). In other words, if a certain set of controller parameters can maintain the small-signal stability of the power grid at the rated wind speed, it can guarantee the stability of the system even above the rated wind speed. By contrast, when the WT runs in the zone AB and zone BC, the output power of the WT and the corresponding characteristic equations vary with the wind speed. The impact of the parameters of the control system on the small-signal stability of the system under different wind speeds must be analyzed in detail.

As the most frequent operational condition and the highest efficiency of the turbine lies in zone CD, we would like to set controller parameters in a way that the largest stability margin Y happens in this zone. However, to maintain the small-signal stability of the grid under all possible wind speed, the selected parameters in zone CD may need to be altered as small as possible to regain the stability in other zones. Therefore, the following controller parameter setting strategy is proposed.

Firstly, a feasible region of the controller parameters is determined according to empirical experiences, and a set of initial parameters is randomly generated within the feasible region. Secondly, participation factors between the controller parameters and eigenvalues are calculated. Then controller parameters are adjusted in a descending order of the participation factors to ensure the small-signal stability of the power grid. Due to the nonlinear nature of the system, the eigenvalue position and the control parameters cannot always be changed synchronously. Therefore, the control parameters adjustment step d cannot be too large. In this paper, we set $d = 0.01$.

The controller parameters setting strategy of the DFIG WT can be further elaborated as follows:

Step 1: Initialization.

Step 1.1: Set the maximum number of iterations to D , and $a = 0$.

Step 1.2: Input the empirical feasible ranges of control parameters

Step 1.3: Randomly initialize parameters K_{pj} ($j = 1, 2, \dots, 6, \beta$) within the feasible ranges

Step 1.4: If $a > D$, go to Step 5.

Step 2: Start with the rated wind speed.

- Calculate eigenvalues λ_i ($i = 1, 2, \dots, N$), participation factors p_{ki} , Y_i , and Y according to equations (37, 43, 41 and 42).
- Sort eigenvalues λ_i ($i = 1, 2, \dots, N$) in ascending order of Y_i and for each λ_i , sort K_{pj} ($j = 1, 2, \dots, M$) in descending order of modulus of p_{ki} , where M is the number of non-zero p_{ki} .
- For each λ_i , successively adjust the control parameters K_{pj} ($j = 1, 2, \dots, M$) within the feasible range (one at a time) to make λ_i move towards left while maximizing Y .
- If the system is stable, go to Step 3, else go to Step 1.3 and $a = a + 1$.

Step 3: Reduce the wind speed as a step of 0.1 m/s.

Step 3.1: Calculate eigenvalues λ_i ($i = 1, 2, \dots, N$), participation factors p_{ki} , Y_i , and Y according to equations (37, 43, 41 and 42).

Step 3.2: If there are unstable eigenvalues, sort the unstable eigenvalues in ascending order of Y_i . For each unstable eigenvalue, control parameters K_{pj} ($j = 1, 2, \dots, M$) are adjusted in the descending order of modulus of p_{ki} ($i = 1, 2, \dots, N$) to make the eigenvalue move into the stable region. If all eigenvalues are stable, go to Step 3.3, otherwise, go to Step 1.3 and $a = a + 1$.

Step 3.3: If the wind speed is greater than or equal to the cut-in wind speed, go to Step 3. Otherwise, go to Step 4.

Step 4: Test. From the rated to the cut-in wind speed, calculate eigenvalues λ_i ($i = 1, 2, \dots, N$) with a decreasing step of 0.1m/s for the wind speed. If all eigenvalues satisfy equation (42), go to step5 and set $a = a + 1$, otherwise, go to Step 1.3 and $a = a + 1$.

Step 5: Output: controller parameters.

VI. CASE STUDY

Taking a DFIG WT with an infinite bus as an example (Fig. 2). The rated power of the WT is 2MW, the cut-in wind speed is 3m/s, the rated wind speed is 10.4m/s, and the cut-out wind speed is 25m/s.

The feasible range and randomly initialized value of the control parameters $K_{p1} \sim K_{p6}, K_{p\beta}$ are reported in Tab. 1.

The eigenvalues in the ascending order of the Y_i at the rated wind speed are shown in Tab. 2. Among them, $\lambda_{1,2}$ is located on the right side of the coordinate system, and Y is 3021.72.

TABLE 1. Initial controller parameters.

Parameter	K_{p1}	K_{p2}	K_{p3}	K_{p4}	K_{p5}	K_{p6}	$K_{p\beta}$
Feasible range	[0.5,6.5]	[9,15]	[0.1,0.38]	[1.5,2.5]	[2,3]	[2,10]	[0.5,8]
Initial value	6	10	0.21	2.5	2.4	3	6

TABLE 2. Eigenvalues with rated wind speed 10.4m/s.

Eigenvalue number	Real part	Imaginary part	Y_i
$\lambda_{1,2}$	0.66	± 0.42	-1.08
$\lambda_{3,4}$	-0.09	± 0.09	0.00
λ_5	-0.05	0	0.05
λ_6	-0.50	0	0.50
$\lambda_{7,8}$	-0.79	± 0.20	0.59
λ_9	-0.80	0	0.80
$\lambda_{10,11}$	-2.82	± 1.85	0.97
λ_{12}	-4.01	0	4.01
λ_{13}	-16.67	0	16.67
λ_{14}	-26.01	0	26.01
λ_{15}	-2973.2	0	2973.2

TABLE 3. Participation factors under rated wind speed.

	x_1	x_2	x_3	x_4	x_5	x_6	x_β
$\lambda_{1,2}$	0.01	0.05	0	0.99	0.71	0	0.01
$\lambda_{3,4}$	0.65	0.55	0.43	0	0	0.55	0
λ_5	0	0	0	0	0	0	1.69
$\lambda_{7,8}$	0	0	0	0	0	2.34	0
λ_9	0	0.15	0	0	0	0	0
$\lambda_{10,11}$	0	0	0.003	2.91	5.87	0	0
λ_{13}	0	0	0.002	0	0	0	0

The participation factors of the state variables $x_1 \sim x_6, x_\beta$ of each eigenvalue are shown in Tab. 3. It should be noted that the participation factors of the eigenvalues 6, 12, 14, 15 and the corresponding control parameters are 0 (omitted in Tab. 3), therefore $\lambda_6, \lambda_{12}, \lambda_{14}, \lambda_{15}$ cannot be modified by simply changing controller parameters.

In order to clearly show the impacts of variable parameters on the eigenvalues, the trajectories of eigenvalues varied with $K_{p_i} (i = 1, 2, \dots, 5)$ are shown in Fig. 6. The trajectories of K_{p6} and $K_{p\beta}$ are ignored as they do not have an influence on the changes of the system stability.

It can be seen from Fig. 6 that the stability and the stability margin of the power system can be altered by changing K_{p_i} , and the trend is similar to that in Tab. 3. It is manifest from Tab. 3 that to make $\lambda_{1,2}$ move to the left, we should adjust the controller parameters in the order of $K_{p4}, K_{p5}, K_{p2}, K_{p1}, K_{p\beta}$ as their values are decreasing correspondingly. The changes of the controller parameters in the given order and their relevant Y values are given in Tab. 4. Tab. 5 shows the eigenvalues after the adjustment of the controller parameters.

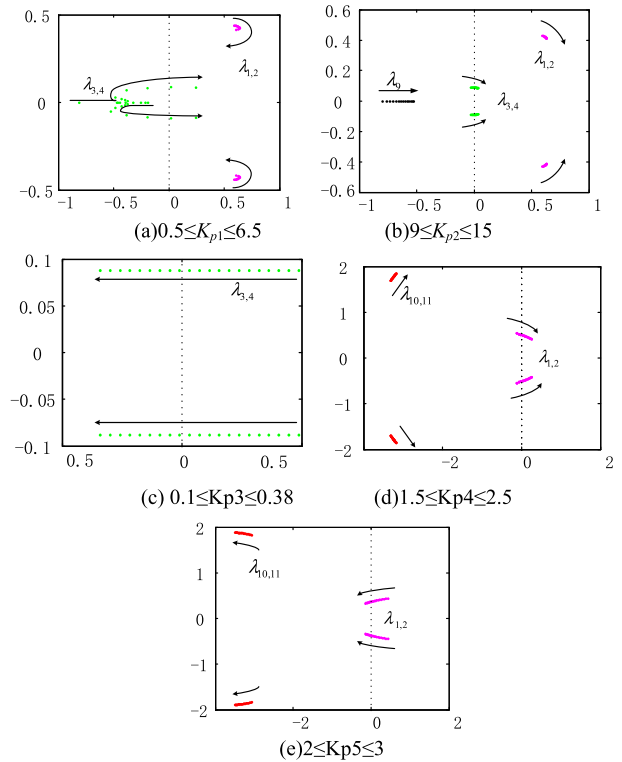


FIGURE 6. The trajectories of eigenvalues with different K_{p_i} under rated wind speed, the arrow pointing to the increase of K_{p_i} . (a) $0.5 \leq K_{p1} \leq 6.5$, (b) $9 \leq K_{p2} \leq 15$, (c) $0.1 \leq K_{p3} \leq 0.38$, (d) $1.5 \leq K_{p4} \leq 2.5$, (e) $2 \leq K_{p5} \leq 3$.

TABLE 4. Process of change of controller parameters for $\lambda_{1,2}$ and the corresponding Y_s .

	K_{p4}	K_{p5}	K_{p2}	K_{p1}	$K_{p\beta}$	K_{p6}	K_{p3}
Value	1.5	3	9	1.2	8	0.5	0.38
Y	3022.2	3022.7	3024.6	3026.2	3026.5	3026.9	3028.5

TABLE 5. Eigenvalues after adjusting parameters for rated wind speed.

Eigenvalue number	Real part	Imaginary part
λ_1	-0.06	0
λ_2	-0.50	0
λ_3	-0.73	0
λ_4	-0.75	0
$\lambda_{5,6}$	-0.82	± 0.28
$\lambda_{7,8}$	-2.11	± 0.51
$\lambda_{9,10}$	-2.61	± 0.17
λ_{11}	-4.01	0
λ_{12}	-4.97	0
λ_{13}	-9.60	0
λ_{14}	-26.01	0
λ_{15}	-2973.2	0

It can be easily seen that after the alteration of the controller parameters, all the eigenvalues for the rated wind speed

TABLE 6. Eigenvalues of the system at the wind speed of 3.8m/s.

Eigenvalue number	Real part	Imaginary part
$\lambda_{1,2}$	0.05	± 0.03
λ_3	-0.50	0
$\lambda_{4,5}$	-0.55	± 0.19
$\lambda_{6,7}$	-1.55	± 0.49
λ_8	-1.69	0
λ_9	-1.76	0
λ_{10}	-2.12	0
λ_{11}	-3.35	0
λ_{12}	-26.01	0
λ_{13}	-2973.2	0

TABLE 7. Non-zero participation factors of $\lambda_{1,2}$ at the wind speed of 3.8m/s.

	x_1	x_2
$\lambda_{1,2}$	0.2204	0.7889

TABLE 8. New controller parameters at the wind speed of 3.8m/s.

	K_{p1}	K_{p2}	K_{p3}	K_{p4}	K_{p5}	K_{p6}	K_{pp}
Value	1	10	0.38	1.5	3	0.5	8

satisfy equation (40) and the Y value also increases along with the changes.

Starting from the controller parameters in Tab. 4, we further reduce the wind speed at a step of 0.1 m/s to check the stability of the grid. The controller parameters can maintain the stability of the power system until the wind speed reduced to 3.8m/s. The eigenvalues of the system at the wind speed of 3.8m/s are given in Tab. 6.

The participation factors of the unstable eigenvalue $\lambda_{1,2}$ are shown in Tab. 7.

The control parameters that can maintain the small-signal stability of the grid at 3.8m/s after adjusting K_{p1} and K_{p2} are given in Tab. 8 and Tab. 9 shows the corresponding eigenvalues.

Similarly, using the proposed method we obtain a new set of controller parameters to regain the small-signal stability of the grid. This new set of controller parameters can maintain system stability until its cut-in speed.

To test the validity of the controller parameters under all wind speeds, we recalculate the eigenvalues of the system from the rated wind speed to the cut-in speed. The trajectories of the eigenvalues are shown in Fig. 7.

It is obvious that with the latest set of controller parameters given in Tab. 8, the turbine does not impose any threat to the stability of the grid under all wind conditions.

TABLE 9. New eigenvalues at the wind speed of 3.8m/s.

Eigenvalue number	Real part	Imaginary part
$\lambda_{1,2}$	-0.550276	± 0.49257
$\lambda_{3,4}$	-0.54767	± 0.1934
λ_5	-0.501	0
λ_6	-0.521071	0
λ_7	-0.5979	0
λ_8	-0.62956	0
λ_9	-1.2392	0
λ_{10}	-3.7677	0
λ_{11}	-26.011	0
$\lambda_{12,13}$	-2973.2	0

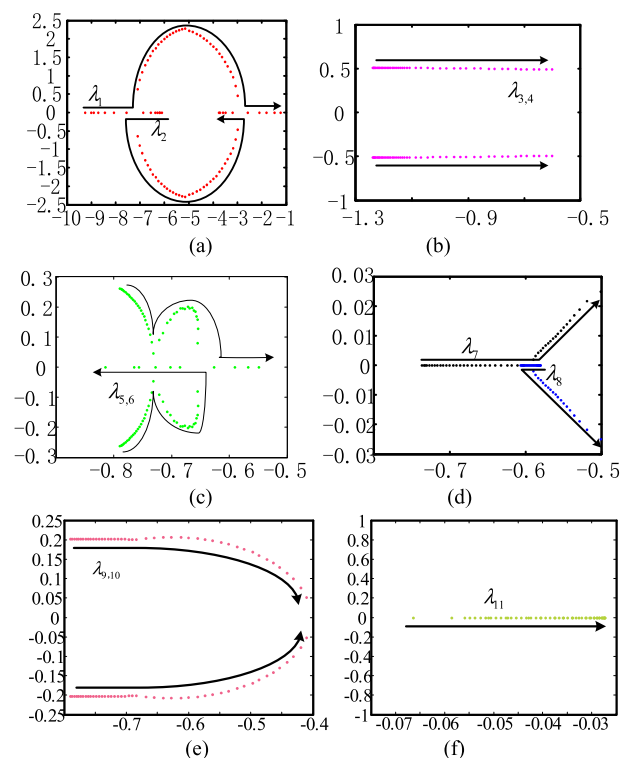


FIGURE 7. Root-locus under different wind speed conditions, the arrow pointing to the increasing of wind speed. (a) Root-locus of $\lambda_{1,2}$, (b) Root-locus of $\lambda_{3,4}$, (c) Root-locus of $\lambda_{5,6}$, (d) Root-locus of $\lambda_{7,8}$, (e) Root-locus of $\lambda_{9,10}$, (f) Root-locus of λ_{11} .

VII. CONCLUSION

The settings of controller parameters to increase the stability of the power system are needed especially with the fast and vast penetration of wind generation in the power system. In this paper, an overall mathematical model of a DFIG WT of direct power control at the rotor-side with an infinite bus system is established for all wind conditions. Based on the in detail analysis of the correlation between the WT controller parameters and the eigenvalues, a WT control system parameters setting strategy considering the small-signal stability of

the grid is proposed, which cannot only guarantee the stability of the system under all wind conditions but also increase the stability margins.

The simulation on a real case shows that there is an inflection point in the trajectory of some eigenvalues as the wind speed changes, and it is impossible to determine universal controller parameters according to the traditional analysis only at a certain wind speed. Control system parameters setting thus must consider the small-signal stability of the grid under all possible wind speed.

The proposed strategy in this paper can maximize the small-signal stability margin of the grid represented by the index Y at the rated wind speed, while at other wind speeds, it can ensure the small-signal stability of the grid by fine-tuning the control parameters. The framework proposed in this paper can provide a theoretical basis for controller parameters setting of wind farms and also have the advantage of simplicity and high efficiency in calculation.

REFERENCES

- [1] D. Zheng, J. Ouyang, X. Xiong, C. Xiao, and M. Li, "A system transient stability enhancement control method using doubly fed induction generator wind turbine with considering its power constraints," *Energies*, vol. 11, no. 4, p. 945, Apr. 2018.
- [2] A. D. Hansen, P. Sørensen, F. Iov, and F. Blaabjerg, "Control of Variable Speed Wind Turbines with Doubly-Fed Induction Generators," *Wind Eng.*, vol. 28, no. 4, pp. 411–432, Jun. 2004.
- [3] A. Tan, X. Lin, J. Sun, R. Lyu, Z. Li, L. Peng, and M. Khalid, "A novel DFIG damping control for power system with high wind power penetration," *Energies*, vol. 9, no. 7, p. 521, Jul. 2016.
- [4] D. Gautam, V. Vittal, and T. Harbour, "Impact of increased penetration of DFIG based wind turbine generators on transient and small signal stability of power systems," *IEEE Trans. Power Systems.*, vol. 24, no. 3, pp. 1426–1434, Aug. 2009.
- [5] O. Aguilar, R. Tapia, A. Valderrabano, and H. Minor, "Design and performance comparison of PI and adaptive current controllers for a WECS," *IEEE Latin Amer. Trans.*, vol. 13, no. 5, pp. 1361–1368, May 2015.
- [6] L. H. Yang, "HOPF bifurcation and eigenvalue sensitivity analysis of doubly fed induction generator wind turbine system," *IEEE PES General Meeting*, vol. 13, no. 5, pp. 1–6, Jul. 2010.
- [7] L. Yang, Z. Xu, J. Østergaard, Z. Y. Dong, K. P. Wong, and X. Ma, "Oscillatory stability and eigenvalue sensitivity analysis of A DFIG wind turbine system," *IEEE Trans. Energy Convers.*, vol. 26, no. 1, pp. 328–339, Mar. 2011.
- [8] B. C. Pal and F. Mei, "Modelling adequacy of the doubly-fed induction generator for small-signal stability studies in power systems," *IET Renew. Power Gener.*, vol. 2, no. 3, pp. 181–190, Jul. 2008.
- [9] S. Ouchen, A. Betka, J. P. Gaubert, and S. Abdeddaim, "Simulation and practical implementation of direct power control applied on PWM rectifier," in *Proc. 6th Int. Conf. Syst. Control (ICSC)*, May 2017, vol. 2, no. 3, pp. 567–571.
- [10] S. K. Salman and A. L. J. Teo, "Windmill modeling consideration and factors influencing the stability of a grid-connected wind power-based embedded generator," *IEEE Power Eng. Rev.*, vol. 18, no. 2, pp. 793–802, May 2003.
- [11] G. Fei, T. Zheng, and Z. Wang, "Comparative study of direct power control with vector control for rotor side converter of DFIG," in *Proc. 9th IET Int. Conf. Adv. Power Syst. Control, Operation Manage. (APSCOM)*, Nov. 2012, vol. 2, no. 3, pp. 181–190.
- [12] C. Wang, Z. Fu, W. Huang, Y. Liu, and S. Zhang, "Doubly-fed wind turbine mathematical model and simulation," in *Proc. Int. Symp. Comput., Consum. Control*, Jun. 2014, vol. 2, no. 3, pp. 793–795.
- [13] Z. Wang, G.-J. Li, Y. Sun, and B. T. Ooi, "Effect of erroneous position measurements in vector-controlled doubly fed induction generator," *IEEE Trans. Energy Convers.*, vol. 25, no. 1, pp. 59–69, Mar. 2010.
- [14] A. K. Gupta, K. Verma, and K. R. Niazi, "Dynamic impact analysis of DFIG-based wind turbine generators on low-frequency oscillations in power system," *IET Gener. Transmiss. Distrib.*, vol. 11, no. 18, pp. 4500–4510, Dec. 2017.
- [15] K. W. Wang, C. Y. Chung, C. T. Tse, and K. M. Tsang, "Multimachine eigenvalue sensitivities of power system parameters," *IEEE Trans. Power Syst.*, vol. 15, no. 2, pp. 741–747, May 2000.



YANBING JIA (Member, IEEE) was born in 1980. She received the B.S. and M.S. degrees in electrical engineering from the Taiyuan University of Technology (TYUT), Shanxi, China, in 2005, and the Ph.D. degree in electrical engineering from Shanghai Jiaotong University, Shanghai, China, in 2009.

From 2009 to 2013, she was an Assistant Professor with TYUT, where she was an Associate Professor, from 2013 to 2018. From 2016 to 2017,

she was a Visitor Researcher with Nanyang Technological University, Singapore. Since 2019, she has been a Professor with the Electrical Engineering Department, TYUT. Her research interests include the operation and planning of the power systems, the influence of new energy to the power systems, and the stability and reliability of the power systems.



TAO HUANG (Member, IEEE) was born in 1980. He received the B.S. and M.S. degrees in electrical engineering from Shanghai Jiaotong University, Shanghai, China, in 2006 and 2002, respectively, and the Ph.D. degree in electrical engineering from the Politecnico di Torino, Turin, Italy, in 2010. He is currently working as a Researcher with the Department of Energy, Politecnico di Torino, and a Professor with the School of Electrical Engineering and Electronic Information, Xihua University.

His research interests include critical infrastructure protection, vulnerability detection and resilience enhancement, electricity markets, and smart grids.



YUBO LI was born in Yuncheng, Shanxi, China, in 1993. He received the B.S. degree in electric engineering from Shanxi University and the M.S. degree in electric engineering from the Taiyuan University of Technology. He is currently an Electric System Protective Relaying Engineer with Yuncheng Power Supply Company, State Grid Corporation of China. His research interests include the stability of the electric systems and electric system protective relaying.



RONGRONG MA was born in Wenshui, Shanxi, in 1994. She received the degree in electrical engineering and automation from Shanxi University, in 2016. She is currently pursuing the master's degree with the Taiyuan University of Technology. Her research content is in the small interference stability of the power systems.

...